Global optimization of an encapsulated Si/SiO2 L3 cavity with a 43 million quality factor

J. P. Vasco (juan.vasco@epfl.ch)
École Polytechnique Fédérale de Lausanne
V. Savona
École Polytechnique Fédérale de Lausanne

Research Article

Keywords: global optimization, encapsulated silicon, fabrication tolerance

Posted Date: February 16th, 2021

DOI: https://doi.org/10.21203/rs.3.rs-197762/v1

Global optimization of an encapsulated Si/SiO_2 L3 cavity with a 43 million quality factor

J.P. Vasco[1,*] **and V. Savona**[1]

[1]Institute of Physics, École Polytechnique Fédérale de Lausanne (EPFL), CH-1015 Lausanne, Switzerland
[*]juan.vasco@epfl.ch

ABSTRACT

We optimize a silica-encapsulated silicon L3 photonic crystal cavity for ultra-high quality factor by means of a global optimization strategy, where the closest holes surrounding the cavity are varied to minimize out-of-plane losses. We find an optimal value of $Q_c = 4.33 \times 10^7$, which is predicted to be in the 2 million regime in presence of structural imperfections compatible with state-of-the-art silicon fabrication tolerances.

Introduction

Photonic crystal (PC) slab cavities have been focus of intense research during the last two decades due to their unique properties to efficiently confine light at length scales close to the diffraction limit, and extremely low loss rates[1,2]. These features have allowed to study a wide variety of classical and quantum phenomena, where the linear and non-linear interactions between light and matter are effectively enhanced in the cavity region[3–20]. Broadly speaking, the strength of this enhancement grows with the local density of electromagnetic states, which is proportional to the quality factor of the cavity mode Q_c, and inversely proportional to its mode volume V[21–23]. Hence, massive efforts have been directed toward the optimization of these figures of merit in order to reach the desired functionality of the photonic device[24–29]. Particularly, silicon-based cavities have attracted very much attention because of their natural compatibility with CMOS technologies and negligible material losses at telecom wavelengths, allowing the integration with optoelectronic devices in a single chip[30]. While free-standing silicon PC slabs offer an excellent platform to build ultralow loss cavities[27,31,32], silica (SiO_2) encapsulation improves the mechanical stability and thermal dissipation of the system[33], while mitigating additional loss channels coming from the etching of air holes in the silicon[34]. Nevertheless, high quality factors are challenging in such encapsulated structures given the low refractive index contrast between the two materials.

In this work, we employ a global optimization approach to maximize the quality factor of a Si/SiO_2 L3 PC cavity. We find an optimal quality factor of $Q_c = 4.33 \times 10^7$, which corresponds to a remarkable low out-of-plane losses given the short length of the cavity. Our results set a new record for the L3 paradigm and open the way to a new class of highly efficient and ultra-compact optical devices for linear and non-linear applications in classical and quantum photonics.

L3 cavity optimization

We consider a silica-encapsulated silicon PC slab with a hexagonal lattice of holes of radii $r = 100$ nm, lattice parameter $a = 390$ nm and thickness $d = 220$ nm. Refractive indices of SiO_2 and Si are taken at telecom wavelengths, i.e., $n_{SiO_2} = 1.44$ and $n_{Si} = 3.47$, respectively. A L3 cavity is introduced by removing three holes along the ΓK direction of the lattice. In order to optimize the quality factor Q_c of its fundamental mode, we adopt a global optimization approach in which only the closest holes surrounding the cavity are varied, in size $r \to r + dr$ and position $(x,y) \to (x+dx, y+dy)$, to reduce out-of-plane losses. This technique has been extremely successful during the last few years to reach record theoretical and experimental quality factors for a wide variety of different materials and cavity geometries[20,25,27,35–38]. Specifically, we employ the particles swarm (PS) algorithm to achieve this goal with Q_c as the objective function and the guided mode expansion method (GME)[39] as the main PC solver. We show in Fig. 1 the schematic representation of the holes to be considered in the optimization procedure, where mirror symmetry with respect to the planes $x = 0$ and $y = 0$ is assumed. Thereby, we end up with a total of 53 optimization parameters. However, after 1400 iterations of the PS algorithm we have noticed that the most relevant parameters for increasing Q_c are those highlighted in red in Fig. 1. This preliminary analysis allowed us to reduce the dimension of the optimization parameter space from 53 to 27, and decrease the number of function evaluations required by the algorithm to converge. We summarize in Table 1 our final results where

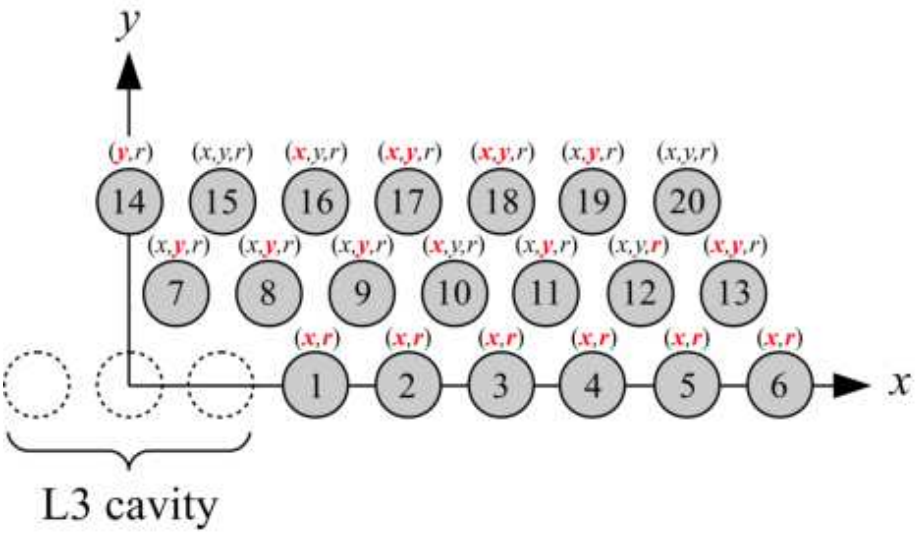

Figure 1. Schematic representation of the closest holes surrounding the L3 cavity, in the first quadrant, which are considered in the global optimization procedure. Mirror symmetry with respect to $x = 0$ and $y = 0$ is assumed, thus setting a total of 53 optimization parameters. Nevertheless, only the ones highlighted in red are found to be the most relevant to increase the fundamental mode quality factor.

Table 1. Summary of the main linear and non-linear figures of merit of the non-optimized and optimized Si/SiO_2 L3 cavities.

Si/SiO_2 – L3 cavity	f (Thz)	Q_c	$V_l\ (\lambda/n_{Si})^3$	$V_{nl}\ (\lambda/n_{Si})^3$	$Q_c/V_l\ (n_{Si}/\lambda)^3$	$Q_c^2/V_{nl}^2\ (n_{Si}/\lambda)^6$
Non-optimized	195.2	1.33×10^3	0.67	3.25	1.99×10^3	1.68×10^5
Optimized	191.2	4.33×10^7	1.75	7.47	2.47×10^7	3.36×10^{13}

$$V_l = \frac{\int \varepsilon(\mathbf{r})|\mathbf{E}(\mathbf{r})|^2 d\mathbf{r}}{\mathrm{Max}\{\varepsilon(\mathbf{r})|\mathbf{E}(\mathbf{r})|^2\}}, \tag{1}$$

is the linear mode volume and

$$V_{nl} = \frac{\left[\int \varepsilon(\mathbf{r})|\mathbf{E}(\mathbf{r})|^2 d\mathbf{r}\right]^2}{\int \varepsilon^2(\mathbf{r})|\mathbf{E}(\mathbf{r})|^4 d\mathbf{r}}, \tag{2}$$

is the non-linear one[40], with $\varepsilon(\mathbf{r})$ representing the dielectric function of the system and $\mathbf{E}(\mathbf{r})$ the electric field of the cavity mode. A global maximum of $Q_c = 4.33 \times 10^7$ (computed with FDTD[41]) is found after 806200 function evaluations, leading to an improvement of four orders of magnitude with respect to the non-optimized cavity. While this theoretical quality factor is around 50% of the record value achieved in glass-clad hetero-structured cavities[42], it corresponds to the largest reported for the encapsulated L3 cavity. Moreover, the short-length mode confinement provided by the L3 geometry is more convenient for applications in ultra-compact devices. It is noteworthy that, Q_c is maximized at the expense of the linear and non-linear mode volumes, in contrast to previous optimizations of the L3 cavity[25]. Nevertheless, we still get extremely large enhancement factors Q_c/V_l and Q_c^2/V_{nl}^2 which are in the 10^7 and 10^{13} regimes, respectively. The increase of the mode volume is clearly seen in the Fig. 2, where we plot the near-field intensity distribution of the fundamental cavity mode in the middle of the slab, for the non-optimized cavity, Fig. 2(a), and the optimized one, Fig. 2(b). The holes which are actually varied are represented by magenta circles in Fig. 2(b). The optimal parameters of the cavity as well as the far-filed projection of the near-field components are reported in the Supplementary Information.

The same optimization strategy can be directly applied to the air-bridge silicon L3 cavity within the same parameter space of dimension 27. For this configuration, we have obtained an FDTD quality factor $Q_c = 1.91 \times 10^8$ which is around 20 times larger than the previous record obtained with deep neural networks[43]. While our optimization requires a much larger number of evaluations to find the global maximum of the objective function, it clearly shows that there is still considerable room for further improvement of these figures of merit when increasing the size of the optimization parameter space, i.e., when allowing more structural parameters to vary. Detailed results for the Si/Air L3 cavity are given in the Supplementary Information.

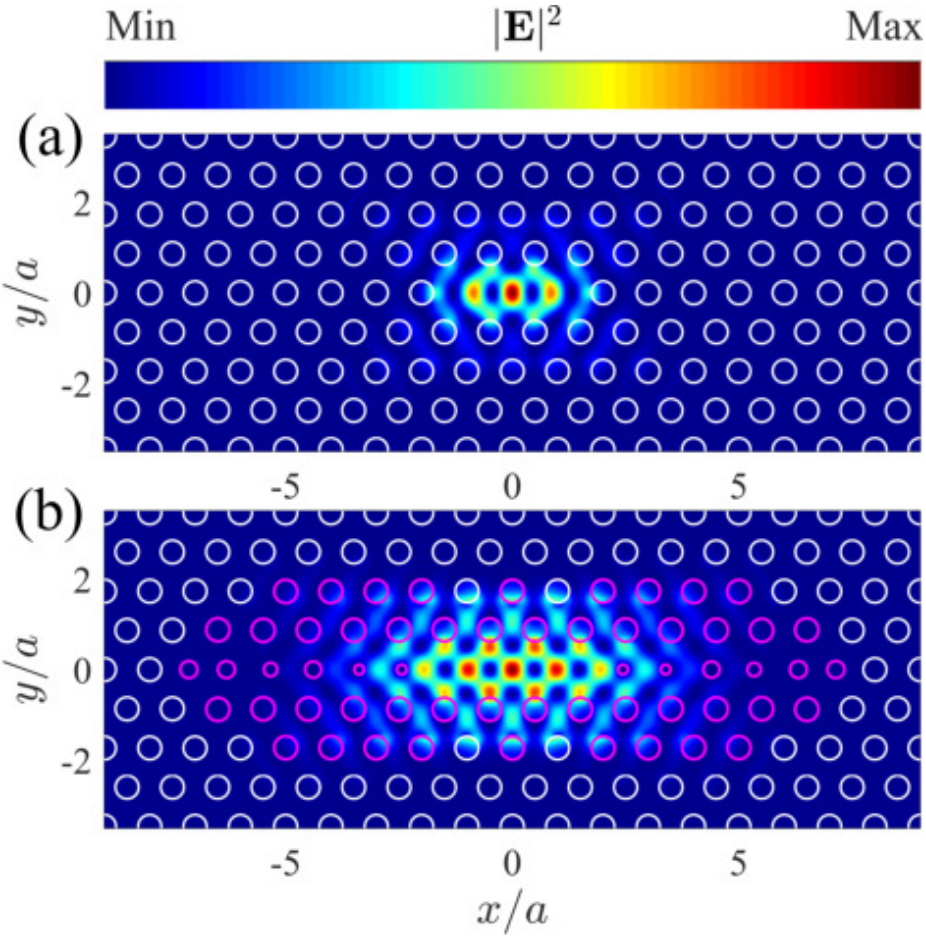

Figure 2. (a) Near-field intensity distribution of the non-optimized L3 fundamental mode cavity. (b) same as (a) for the optimized L3 cavity, where the holes which are actually considered in the optimization are represented by magenta circles.

Disorder analysis

Realistic photonic devices are always subject to a small amount of intrinsic disorder, coming from unavoidable imperfections introduced at the fabrication stage. We model such effect by considering random Gaussian fluctuations in all hole positions and sizes of our PC, where the standard deviation of the Gaussian probability distribution σ is taken as the disorder parameter[44–46]. Results of this analysis are shown in Fig. 3, where the averaged cavity quality factor $\langle Q_c \rangle$, computed over 100 independent disorder realization of the system, is plotted as a function of σ. Typical tolerances in silicon state-of-the-art fabrication techniques range between $\sigma = 0.001a$ and $\sigma = 0.002a$[31,47], which leads to an averaged Q_c in the 2 million regime. Previous measured Q values on 2D PC slab cavities with low index claddings range from 0.6×10^6 (silica cladding)[48] to 1×10^6 (glass cladding)[42], with estimated disorder magnitudes larger than $\sigma = 0.002a$. However, the confinement mechanism is based on hetero-structured PCs waveguides or effective photonic potentials which usually require a long-length cavity region, i.e., more than 20 periods of the underlying photonic lattice.

Conclusions

In conclusion, we have optimized a silica-encapsulated silicon L3 cavity by means of a global optimization strategy, where the closest holes surrounding the cavity are varied to decrease out-of-plane losses. We have found a value of $Q_c = 4.33 \times 10^7$, corresponding to outstanding result given the short-length of the confinement region. To better relate our optimal design to realistic samples, we have also studied the effects of intrinsic disorder. When considering typical tolerances in modern fabrication techniques, the averaged quality factor of the optimized cavity remains in the 2 million regime, which is comparable to previous measurements in fully embedded hetero-structured and photonic potential based designs. Apart from setting a new record for the encapsulated L3 cavity, our results open the way to a new class of optimized designs in low-index-contrast

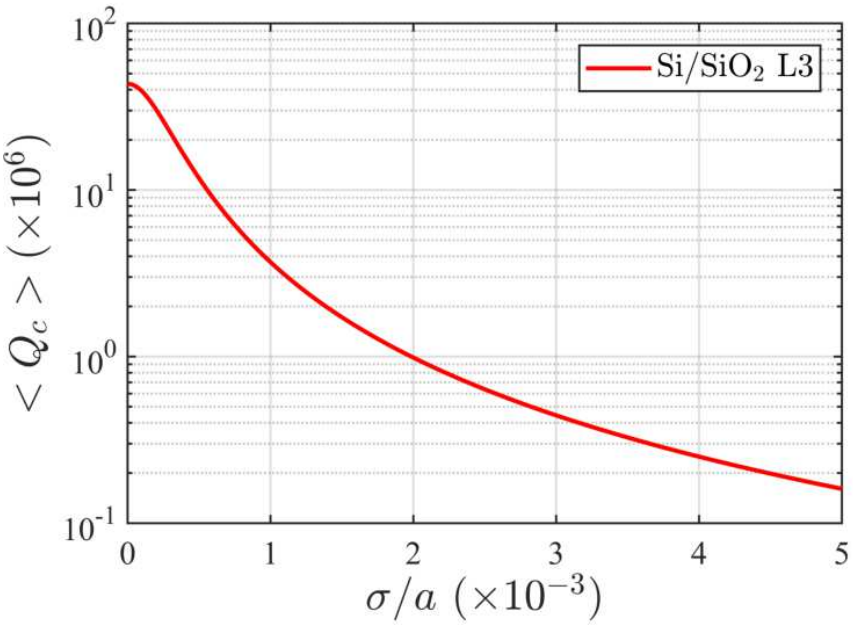

Figure 3. Averaged Q_c, computed over 100 independent disorder realizations of the optimal cavity, as a function of the disorder parameter σ.

materials, such as AlN, GaN or Si_3N_4, holding great promise for nonlinear optical enhancement, sensing, and solid-state quantum optics.

Methods

The guided mode expansion

We employ the guided mode expansion method (GME)[39] as our main PC solver for estimating the cavity mode frequencies and quality factors at the optimization stage. The expansion was carried out in a supercell of dimensions $20a \times 7\sqrt{3}a$ with 8517 plane waves and one TE guided mode. During the optimization procedure we mainly focus on the growing direction of Q_c within the high-dimensional space of parameters. Therefore, only one k point is needed (in the Brillouin zone of the supercell) to compute the real $\Re\{\omega_c\}$ and imaginary $\Im\{\omega_c\}$ parts of the mode frequencies ω_c. The cavity quality factor, associated to out-of-plane losses, is thus defined as

$$Q_c = \frac{\Re\{\omega_c\}}{2\Im\{\omega_c\}} \tag{3}$$

Particles Swarm algorithm

We have used the Particles Swarm (PS) algorithm available in the Global Optimization Toolbox of MATLAB, which starts from a random swarm of 139 particles and requires 5800 iterations to converge. Every particle at each iteration correspond to an independent evaluation of Q_c with GME, thus leading to a total number of 806200 GME simulations to find the global maximum of the objective function Q_c.

FDTD numerical experiments

Once the optimal parameters are found by the PS optimization, we simulate the final structure with a commercial FDTD solver[41]. The cavity mode is excited with an electric dipole oriented along the dominant mode polarization E_y. This source was set to be a standard Gaussian pulse, centered at the cavity frequency with a narrow bandwidth of 0.88 THz. The total size of the PC structure was $86a \times 75\sqrt{3}a/2$ with the L3 cavity localized at the center of the computational cell. PML boundary conditions and mirror symmetry with respect to the planes $x = 0$, $y = 0$ and $z = 0$ were assumed. Finally, maximum mesh steps of $a/40$ and $0.5\sqrt{3}a/40$ were considered along x and y directions, respectively, while 40 cells per wavelength with a grading factor of 1.41421 were set along the z direction.

References

1. Vahala, K. J. Optical microcavities. *Nature* **424**, 839 (2003).
2. Akahane, Y., Asano, T., Song, B.-S. & Noda, S. High-q photonic nanocavity in a two-dimensional photonic crystal. *Nature* **425**, 944 (2003).
3. Yoshie, T. *et al.* Vacuum rabi splitting with a single quantum dot in a photonic crystal nanocavity. *Nature* **432**, 200 (2004).
4. Englund, D. *et al.* Controlling the spontaneous emission rate of single quantum dots in a two-dimensional photonic crystal. *Phys. Rev. Lett.* **95**, 013904 (2005).
5. Hennessy, K. *et al.* Quantum nature of a strongly coupled single quantum dot–cavity system. *Nature* **445**, 896 (2007).
6. Noda, S., Fujita, M. & Asano, T. Spontaneous-emission control by photonic crystals and nanocavities. *Nat. Photonics* **1**, 449 (2007).
7. Faraon, A. *et al.* Coherent generation of non-classical light on a chip via photon-induced tunnelling and blockade. *Nat. Phys.* **4**, 859 (2008).
8. O'Brien, J. L., Furusawa, A. & Vučković, J. Photonic quantum technologies. *Nat. Photonics* **3**, 687 (2009).
9. Rivoire, K., Lin, Z., Hatami, F., Masselink, W. T. & Vučković, J. Second harmonic generation in gallium phosphide photonic crystal nanocavities with ultralow continuous wave pump power. *Opt. Express* **17**, 22609 (2009).
10. Husko, C. *et al.* Ultrafast all-optical modulation in gaas photonic crystal cavities. *Appl. Phys. Lett.* **94**, 021111 (2009).
11. Nomura, M., Kumagai, N., Iwamoto, S., Ota, Y. & Arakawa, Y. Laser oscillation in a strongly coupled single-quantum-dot–nanocavity system. *Nat. Phys.* **6**, 279 (2010).
12. Nozaki, K. *et al.* Sub-femtojoule all-optical switching using a photonic-crystal nanocavity. *Nat. Photonics* **4**, 477 (2010).
13. Galli, M. *et al.* Low-power continuous-wave generation of visible harmonics in silicon photonic crystal nanocavities. *Opt. Express* **25**, 26613 (2010).
14. Ellis, B. *et al.* Ultralow-threshold electrically pumped quantum-dot photonic-crystal nanocavity laser. *Nat. Photonics* **5**, 297 (2011).
15. Reinhard, A. *et al.* Strongly correlated photons on a chip. *Nat. Photonics* **6**, 93 (2012).
16. Nozaki, K. *et al.* Ultralow-power all-optical ram based on nanocavities. *Nat. Photonics* **6**, 248 (2012).
17. Volz, T. *et al.* Ultrafast all-optical switching by single photons. *Nat. Photonics* **6**, 605 (2012).
18. Shakoor, A. *et al.* Room temperature all-silicon photonic crystal nanocavity light emitting diode at sub-bandgap wavelengths. *Laser Photonics Rev.* **7**, 114 (2013).
19. Takahashi, Y. *et al.* A micrometre-scale raman silicon laser with a microwatt threshold. *Nature* **498**, 470 (2013).
20. Dharanipathy, U. P., Minkov, M., Tonin, M., Savona, V. & Houdré, R. High-q silicon photonic crystal cavity for enhanced optical nonlinearities. *Appl. Phys. Lett.* **105**, 101101 (2014).
21. Yao, P., Rao, V. M. & Hughes, S. On-chip single photon sources using planar photonic crystals and single quantum dots. *Laser Photonics Rev.* **4**, 499 (2010).
22. Kristensen, P. T. & Hughes, S. Modes and mode volumes of leaky optical cavities and plasmonic nanoresonators. *ACS Photonics* **1**, 2 (2014).
23. Vasco, J. & Hughes, S. Anderson localization in disordered ln photonic crystal slab cavities. *ACS Photonics* **5**, 1262 (2018).
24. Chalcraft, A. R. A. *et al.* Mode structure of the l3 photonic crystal cavity. *Appl. Phys. Lett.* **90**, 241117 (2007).
25. Minkov, M. & Savona, V. Automated optimization of photonic crystal slab cavities. *Sci. Rep.* **4**, 5124 (2014).
26. Tanaka, Y., Asano, T. & Noda, S. Design of photonic crystal nanocavity with q-factor of 10^9. *J. Light. Technol* **26**, 1532 (2008).
27. Minkov, M., Savona, V. & Gerace, D. Photonic crystal slab cavity simultaneously optimized for ultra-high q/v and vertical radiation coupling. *Appl. Phys. Lett.* **111**, 131104 (2017).
28. Asano, T. & Noda, S. Optimization of photonic crystal nanocavities based on deep learning. *Opt. Express* **26**, 32704 (2018).

29. Minkov, M., Gerace, D. & Fan, S. Doubly resonant $\chi^{(2)}$ nonlinear photonic crystal cavity based on a bound state in the continuum. *Optica* **6**, 1039 (2019).

30. Wang, J. & Long, Y. On-chip silicon photonic signaling and processing: a review. *Sci. Bull.* **63**, 1267 (2018).

31. Asano, T., Ochi, Y., Takahashi, Y., Kishimoto, K. & Noda, S. Photonic crystal nanocavity with a q factor exceeding eleven million. *Opt. Express* **25**, 1769 (2017).

32. Simbula, A. *et al.* Realization of high-q/v photonic crystal cavities defined by an effective aubry-andré-harper bichromatic potential. *APL photonics* **2**, 056102 (2017).

33. Bazin, A. *et al.* Thermal management in hybrid inp/silicon photonic crystal nanobeam laser. *Opt. Express* **22**, 10570 (2014).

34. Borselli, M., J. Johnson, T. & Painter, O. Measuring the role of surface chemistry in silicon microphotonics. *Appl. Phys. Lett.* **88**, 131114 (2006).

35. Lai, Y. *et al.* Genetically designed l3 photonic crystal nanocavities with measured quality factor exceeding one million. *Appl. Phys. Lett.* **104**, 241101 (2014).

36. Triviño, N. V. *et al.* Gallium nitride l3 photonic crystal cavities with an average quality factor of 16 900 in the near infrared. *Appl. Phys. Lett.* **105**, 231119 (2014).

37. Flayac, H., Minkov, M. & Savona, V. Remote macroscopic entanglement on a photonic crystal architecture. *Phys. Rev. A* **92**, 043812 (2015).

38. Vasco, J., Gerace, D. & Savona, V. Optimized design of a silica encapsulated photonic crystal nanobeam cavity for integrated silicon-based nonlinear and quantum photonics. *arXiv:1910.10647* (2019).

39. Andreani, L. C. & Gerace, D. Photonic-crystal slabs with a triangular lattice of triangular holes investigated using a guided-mode expansion method. *Phys. Rev. B* **73**, 235114 (2006).

40. Barclay, P. E., Kartik, S. & Painter, O. Nonlinear response of silicon photonic crystal microresonators excited via an integrated waveguide and fiber taper. *Opt. Express* **13**, 801 (2005).

41. *Lumerical Solutions, Inc.* https://www.lumerical.com/tcad–products/fdtd/.

42. Song, B.-S., Jeon, S.-W. & Noda, S. Symmetrically glass-clad photonic crystal nanocavities with ultrahigh quality factors. *Opt. Lett.* **36**, 91 (2011).

43. Asano, T. & Noda, S. Iterative optimization of photonic crystal nanocavity designs by using deep neural networks. *arXiv:1908.03702* (2019).

44. Gerace, D. & Andreani, L. C. Disorder-induced losses in photonic crystal waveguides with line defects. *Opt. Lett.* **29**, 1897 (2004).

45. Minkov, M., Dharanipathy, U. P., Houdré, R. & Savona, V. Statistics of the disorder-induced losses of high-q photonic crystal cavities. *Opt. Express* **21**, 28233 (2013).

46. Vasco, J. & Savona, V. Disorder effects on the coupling strength of coupled photonic crystal slab cavities. *New J. Phys.* **20**, 075002 (2018).

47. Mohamed, M. S. *et al.* Influence of disorder and finite-size effects on slow light transport in extended photonic crystal coupled-cavity waveguides. *ACS Photonics* **5**, 4846 (2018).

48. Dodane, D., Bourderionnet, J., Combrié, S. & de Rossi, A. Fully embedded photonic crystal cavity with q=0.6 million fabricated within a full-process cmos multiproject wafer. *Opt. Express* **26**, 20868 (2018).

Author contributions statement

J.P. Vasco and V. Savona equally contributed to the simulation and analysis of all results, as well as the preparation of the manuscript.

Additional information

Competing interests

The authors declare no competing interests.

Figures

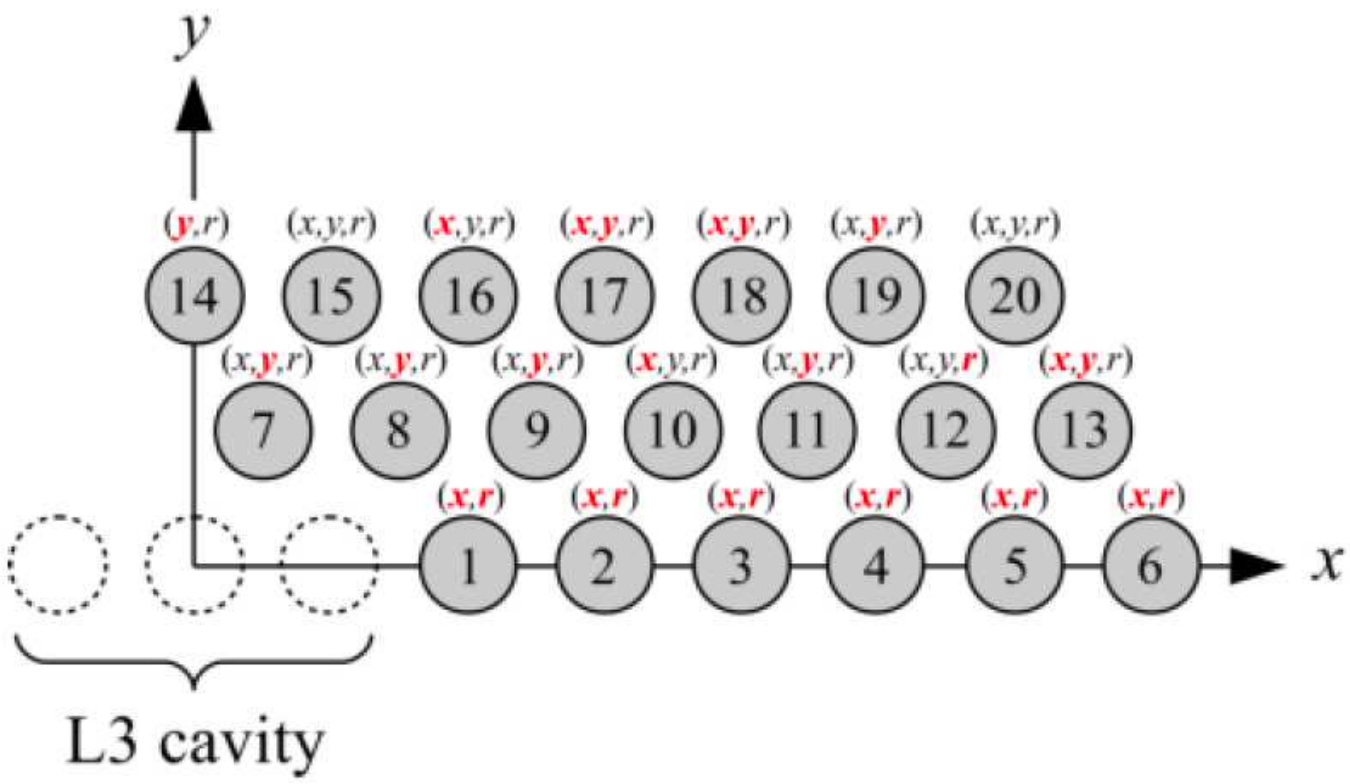

Figure 1

Schematic representation of the closest holes surrounding the L3 cavity, in the first quadrant, which are considered in the global optimization procedure. Mirror symmetry with respect to x = 0 and y = 0 is assumed, thus setting a total of 53 optimization parameters. Nevertheless, only the ones highlighted in red are found to be the most relevant to increase the fundamental mode quality factor.

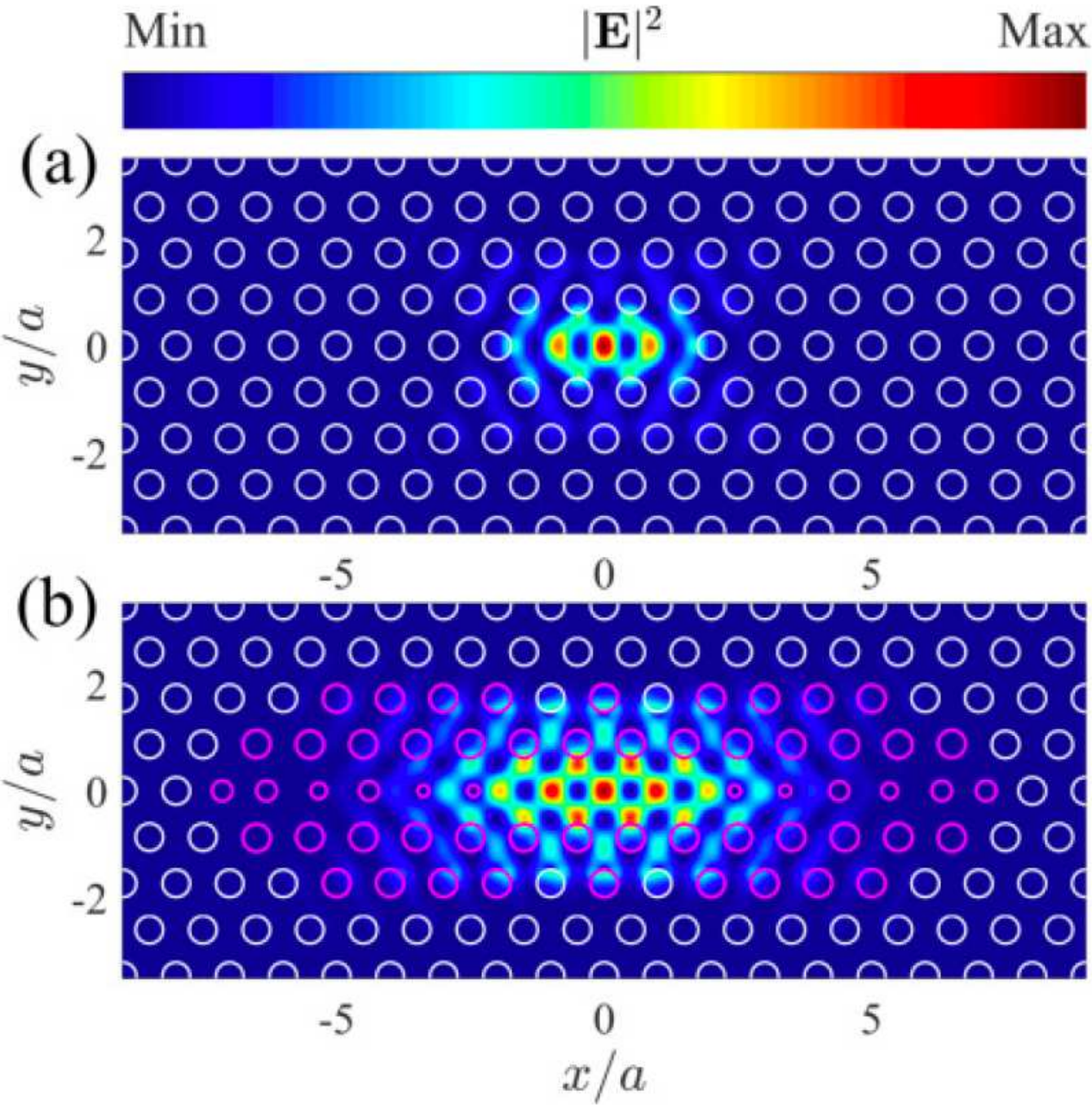

Figure 2

(a) Near-field intensity distribution of the non-optimized L3 fundamental mode cavity. (b) same as (a) for the optimized L3 cavity, where the holes which are actually considered in the optimization are represented by magenta circles.

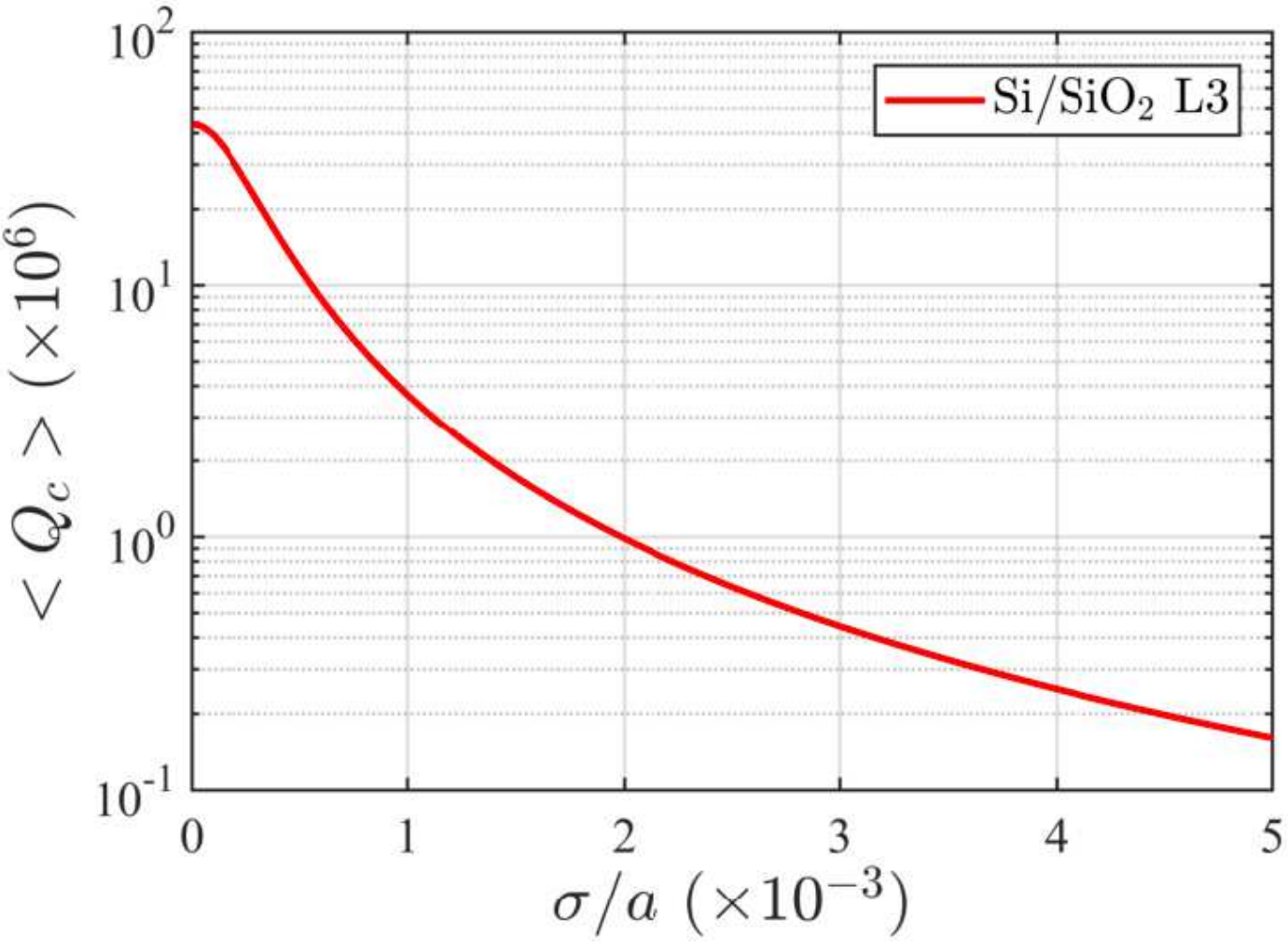

Figure 3

Averaged Qc, computed over 100 independent disorder realizations of the optimal cavity, as a function of the disorder parameter σ.

Supplementary Files

This is a list of supplementary files associated with this preprint. Click to download.

- Supplementaryinformation.pdf